Water Uptake along the Length of Grapevine Fine Roots: Developmental Anatomy, Tissue-Specific Aquaporin Expression, and Pathways of Water Transport[1][W][OPEN]

Gregory A. Gambetta, Jiong Fei, Thomas L. Rost, Thorsten Knipfer, Mark A. Matthews, Ken A. Shackel, M. Andrew Walker, and Andrew J. McElrone*

Department of Viticulture and Enology (G.A.G., J.F., T.K., M.A.M., M.A.W., A.J.M.), Department of Plant Biology (T.L.R.), and Department of Plant Science (K.A.S.), University of California, Davis, California 95616; and United States Department of Agriculture-Agricultural Research Service, Crops Pathology and Genetics Research Unit, Davis, California 95616 (A.J.M.)

To better understand water uptake patterns in root systems of woody perennial crops, we detailed the developmental anatomy and hydraulic physiology along the length of grapevine (*Vitis berlandieri* × *Vitis rupestris*) fine roots from the tip to secondary growth zones. Our characterization included the localization of suberized structures and aquaporin gene expression and the determination of hydraulic conductivity (Lp_r) and aquaporin protein activity (via chemical inhibition) in different root zones under both osmotic and hydrostatic pressure gradients. Tissue-specific messenger RNA levels of the plasma membrane aquaporin isogenes (*VvPIP*s) were quantified using laser-capture microdissection and quantitative polymerase chain reaction. Our results highlight dramatic changes in structure and function along the length of grapevine fine roots. Although the root tip lacked suberization altogether, a suberized exodermis and endodermis developed in the maturation zone, which gave way to the secondary growth zone containing a multilayer suberized periderm. Longitudinally, *VvPIP* isogenes exhibited strong peaks of expression in the root tip that decreased precipitously along the root length in a pattern similar to Arabidopsis (*Arabidopsis thaliana*) roots. In the radial orientation, expression was always greatest in interior tissues (i.e. stele, endodermis, and/or vascular tissues) for all root zones. High Lp_r and aquaporin protein activity were associated with peak *VvPIP* expression levels in the root tip. This suggests that aquaporins play a limited role in controlling water uptake in secondary growth zones, which contradicts existing theoretical predictions. Despite having significantly lower Lp_r, woody roots can constitute the vast majority of the root system surface area in mature vines and thus provide for significant water uptake potential.

In woody perennial root systems, the majority of water uptake is often attributed to unsuberized fine roots (Kramer and Boyer, 1995), even though woody portions can constitute the vast majority of root surface area for these plants at maturity (Nightingale, 1934; Kramer and Bullock, 1966). This assumption has likely been reinforced by the fact that most studies investigating root water uptake have been done with herbaceous species, whose roots function more like the tips of woody perennials. Although unsuberized fine roots typically have a greater ability to absorb water (i.e. they are more conductive per unit of surface area), it has been shown that older suberized portions of woody taproots can still contribute significantly to root system water uptake (Kramer and Bullock, 1966; Queen, 1967; Chung and Kramer, 1975; MacFall et al., 1990, 1991). Despite this knowledge and the fact that unsuberized roots of many woody perennials are scarce or absent during periods of the growing season when peak transpiration requires much water (MacFall et al., 1991), we still know little about how suberized portions of perennial rooting systems contribute to radial water absorption across species.

The composite transport model (Steudle, 2001) is a conceptual framework describing water transport into plant roots. This model posits that water is able to flow into the root via multiple parallel pathways, traveling either in the cell walls (apoplastic) and/or from cell to cell (symplastic and/or transcellular). Transport across the cell-to-cell pathway can involve water crossing plasma membranes; thus, the rate of water uptake can be influenced by the abundance and activity of aquaporins (i.e. water channels). The contribution of aquaporins to root water uptake has been the focus of numerous

[1] This work was supported by a National Institute of Food and Agriculture-Specialty Crops Research Initiative grant and funding from the American Vineyard Foundation to A.J.M. and by the U.S. Department of Agriculture-Agricultural Research Service Current Research Information System (research project no. 5306–21220–004–00).

* Address correspondence to ajmcelrone@ucdavis.edu.

The author responsible for distribution of materials integral to the findings presented in this article in accordance with the policy described in the Instructions for Authors (www.plantphysiol.org) is: Andrew J. McElrone (ajmcelrone@ucdavis.edu).

[W] The online version of this article contains Web-only data.

[OPEN] Articles can be viewed online without a subscription.

www.plantphysiol.org/cgi/doi/10.1104/pp.113.221283

studies, and the absolute magnitude of this contribution appears to be highly variable, ranging from 20% to 90% across species (for review, see Javot and Maurel, 2002). Steudle (2000) suggested that radial water flow would be dominated by aquaporin regulation in heavily suberized roots, as flow through the apoplast would be minimized. The localization of aquaporins should play a critical role in defining their impact on radial water uptake across suberized and unsuberized roots. For herbaceous species, peak aquaporin mRNA and/or protein levels have been found in root tips and the endodermis, pericycle, phloem, and xylem tissues (Schäffner, 1998; Otto and Kaldenhoff, 2000; Suga et al., 2003; Fraysse et al., 2005; Knipfer et al., 2011). Few aquaporin localization studies have been conducted in woody perennials (Vandeleur et al., 2009). Recent work from our laboratory revealed a precipitous drop in aquaporin expression between the grapevine (*Vitis* spp. rootstocks) root tips and older root portions (Gambetta et al., 2012). These observations led to this study, where we explore patterns of aquaporin localization in *Vitis* species fine roots and how they intersect with the structural anatomy and patterns of suberization to affect water uptake along the root length.

Hydraulic conductivity (Lp_r) of the apoplastic pathway can be altered through changes in cell wall chemistry, especially through the deposition of suberin. Suberized apoplastic barriers in plant roots include the Casparian band of the endodermis and the suberin lamella of the endodermis, exodermis, and periderm in woody species (Esau, 1977). Casparian bands and suberin lamella are solute impermeable (for review, see Peterson and Enstone, 1996), but across studies, the extent to which they impede the flow of water is highly variable (Peterson et al., 1993; Steudle et al., 1993; Peterson and Enstone, 1996; Schreiber et al., 2005). Regardless, studies support the idea that in roots there is always some flow across the cell-to-cell pathway due to apoplastic barriers and/or an osmotic component to the driving gradient (Steudle et al., 1993; Miyamoto et al., 2001; Knipfer and Fricke, 2011). In the cell-to-cell pathway, Lp_r can be altered by intrinsic plasma membrane properties, plasmodesmata (Oparka and Prior, 1992; Roberts and Oparka, 2003), and/or the abundance and activity of aquaporins. Changes in aquaporin gene expression and protein activity remain potentially dynamic and can occur within hours, while alterations of suberized apoplastic barriers are permanent and would manifest over longer developmental time frames.

The total water potential gradient across a fine root can be composed of both osmotic ($\Delta\Psi^{Os}$) and hydrostatic ($\Delta\Psi^{Hy}$) pressure gradients. A purely $\Delta\Psi^{Os}$ requires that some portion of the pathway be cell to cell. A purely $\Delta\Psi^{Hy}$ should drive flow through both pathways, and the proportion of flow through the two pathways will be determined by their Lp_r. Experimentally, Lp_r generated under $\Delta\Psi^{Hy}$ is typically greater than Lp_r generated under $\Delta\Psi^{Os}$, typically ranging from 2-fold to more than 100-fold greater (Steudle et al., 1987; Hallgren et al., 1994; Miyamoto et al., 2001; Knipfer and Fricke, 2011). In some cases, Lp_r is nearly equal under both types of gradients (Miyamoto et al., 2001; Knipfer and Fricke, 2011). These results suggest that if Lp_r through the apoplast were to be reduced by the presence of an apoplastic barrier, this would force flow across a cell-to-cell pathway regardless of the driving gradient (Steudle, 2000).

In this study, we sought to provide a more detailed understanding of the localization of aquaporin expression and its contribution to radial water uptake in different zones of grapevine fine roots, from the unsuberized actively growing root tip to portions of the fine root undergoing secondary growth and containing a developed periderm. We characterized the developmental anatomy along the length of the fine root, including the localization of suberized structures, and quantified tissue-specific mRNA levels of plasma membrane aquaporin isogenes via a combination of laser-capture microdissection (LCM) and quantitative PCR. Finally, we determined the Lp_r of root tips and secondary growth root zones under both $\Delta\Psi^{Os}$ and $\Delta\Psi^{Hy}$ while investigating the contribution of aquaporin activity to Lp_r via chemical inhibition.

RESULTS

Developmental Anatomy

For our analysis of the developmental anatomy, we delimit the fine root into three zones: the meristematic/elongation zone (i.e. the tip), the maturation zone, and the secondary growth zone. Grape roots exhibited a developmental pattern common to woody perennials; the meristematic and elongation zones typically extended to distances of 10 to 30 mm from the root apex (Fig. 1), and tissues within this zone remained undifferentiated (Fig. 1, A–C). The maturation zone initiated at distances of approximately 40 mm or greater from the root tip, where the primary xylem, primary phloem, and endodermis differentiated (Fig. 1, D–H). The majority of roots examined contained four primary xylem poles in the maturation zone (tetrarch; Fig. 1, D–F), but others regularly contained triarch or pentarch patterns. At distances of more than 100 mm, secondary growth was initiated (Fig. 1, I–L); in this zone, the vascular cambium formed and gave rise to secondary xylem and phloem tissues (Fig. 1, I and J). In the oldest root portions examined here, the arch nature of the xylem poles was lost, the periderm formed from the outer layers of the pericycle, and the outer cell layers containing the exodermis, cortex, and endodermis began to break down and rupture (Fig. 1, K and L). In older more distal root zones, all cell layers residing outside of the periderm were lost. Along the length of the root, the cortex thickness, as a percentage of the root diameter, was constant up to distances greater than 150 mm from the apex, where it decreased until rupture occurred (data not shown).

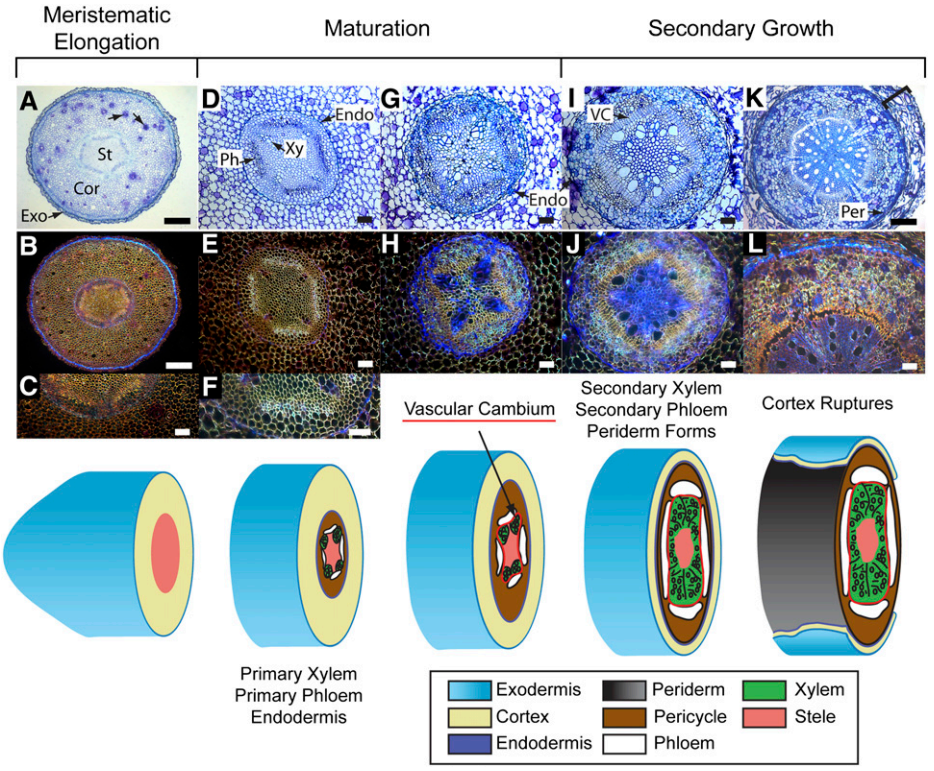

Figure 1. Developmental anatomy of grapevine fine roots visualized through the use of bright- and dark-field microscopy. A to C, Undifferentiated tissue of the meristematic and elongation zones: exodermis (Exo), cortex (Cor), and stele (St). Dark blotches in A (black arrows) are raphides. D to H, Maturation zone including the appearance of primary xylem (Xy), primary phloem (Ph), and an identifiable endodermis (Endo). I to L, Secondary growth with the vascular cambium (VC) clearly visible. At later stages (K and L), the periderm (Per) forms and the exodermis, cortex, and endodermis rupture and are lost (bracketed in K). Bars = 200 μm (A, B, and K), 40 μm (F), and 80 μm (all others).

The variability of suberized structures was apparent along the length of fine roots as visualized using berberine sulfate, analine blue staining (Fig. 2). No suberized layers were detected in the meristematic and elongation zones (Fig. 2, A and B). Coincident with the first appearance of primary xylem was the presence of a fully developed Casparian band in the endodermis and a suberized exodermis in the maturation zone (Fig. 2C). At this location, the exodermis was suberized on both anticlinal walls and the interior periclinal wall (Fig. 2C, inset) and also contained sections, typically one to three cells wide, where no suberization was detected (i.e. passage cells; Vandeleur et al., 2009). As primary xylem developed, these suberization patterns remained consistent, except that passage cells in the exodermis were no longer detected in older root zones

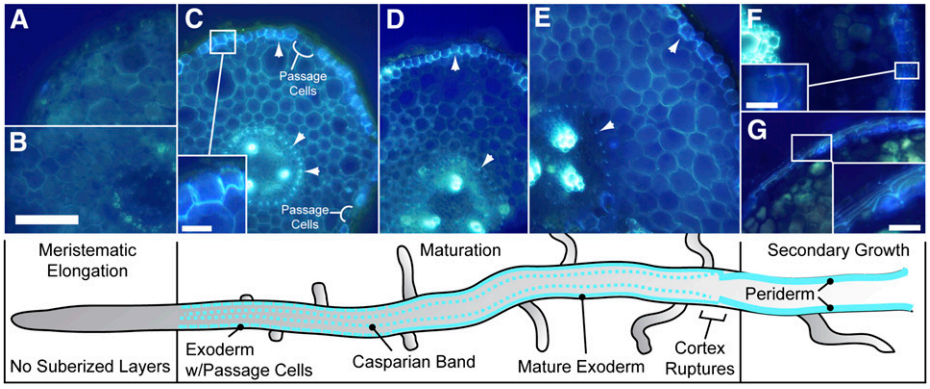

Figure 2. Patterns of suberization along the length of grapevine fine roots visualized through berberine sulfate, analine blue staining. A and B, No suberization was detected within the meristematic and elongation zones. C to E, Within the maturation zone, suberization in both the endodermis and exodermis appeared coincidently (white arrowheads). The exoderm was suberized on both anticlinal, but only the interior periclinal, walls (inset in C). At early stages of development, the suberization in the exodermis was incomplete (passage cells in C). F and G, after the initiation of secondary growth and the rupture and loss of the outer cell layers, there was a multiple cell layer periderm within which both anticlinal and periclinal walls were suberized (insets). Bars = 100 μm (main panels) and 20 μm (insets).

(Fig. 2, D and E). After secondary growth was initiated and the outer cell layers were lost, the resulting periderm contained multiple suberized cell layers (Fig. 2, F and G). The periderm exhibited a suberization pattern similar to the exodermis in that the anticlinal walls were suberized; however, in the periderm, both periclinal walls were suberized (Fig. 2, F and G, insets).

Root Zone Hydraulic Conductivity

Quantification of Lp_r and aquaporin activity revealed significant differences with different driving gradients and across the zones (tips versus secondary growth zones; Fig. 3). Within both root zones, Lp_r under $\Delta\Psi^{Hy}$ (Lp_r^{Hy}) was at least 100-fold greater than Lp_r under $\Delta\Psi^{Os}$ (Lp_r^{Os}; Fig. 3A). When comparing zones, both Lp_r^{Hy} and Lp_r^{Os} were approximately 10 times greater in the meristematic and elongation zones when compared with the secondary growth zone. When aquaporin activity was inhibited, Lp_r^{Os} decreased on average 45% in the meristematic and elongation zones but only 5% in the secondary growth zone (Fig. 3B). Inhibition had very little effect on Lp_r^{Hy}, decreasing 5% in the meristematic and elongation zones while remaining unchanged in the secondary growth zone.

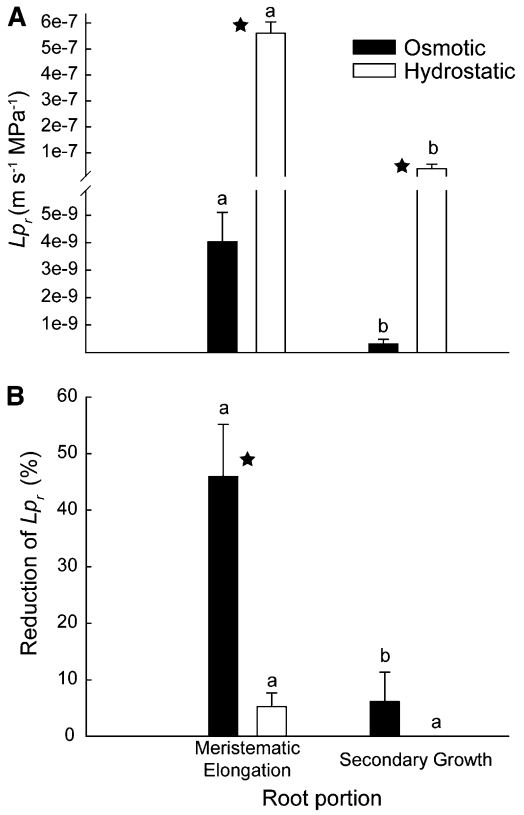

Figure 3. Root portion-specific Lp_r and aquaporin inhibition in *Vitis* species fine roots. A, Root portion Lp_r obtained by using either an osmotic (black bars) or hydrostatic (white bars) driving gradient. B, Percentage reduction in Lp_r for both driving gradients when aquaporins were inhibited with 0.6 mM hydrogen peroxide. Error bars represent SE. Different letters represent significant differences between root portions within a driving gradient, whereas stars represent significant differences between driving gradients within a root portion ($n = 5–7$; Student's t test, $P < 0.05$).

Radial Patterns of *VvPIP* Expression

Tissue-specific mRNA levels for the *Vitis* species plasma membrane aquaporin (*VvPIP*) isogenes varied significantly between tissue types within different root zones (Fig. 4). In the meristematic and elongation zones, the exodermis, cortex, and stele were dissected (Fig. 4A). In this zone, mRNA levels of all isogenes were lowest in the exodermis, with significantly higher levels in the cortex and stele (Fig. 4, B and C). Within the *VvPIP1* family, *VvPIP1-2;1-4* was the most prominently expressed isogene, with mRNA levels approximately 2^3 to 2^6 (note $\log_2$ scale in Fig. 4) greater than the other *VvPIP1* isogenes (Fig. 4B). *VvPIP1-2;1-4* mRNA levels were 16-fold greater in the cortex and stele than in the exodermis, a pattern common to the other *VvPIP1* isogenes. Within the *VvPIP2* family, *VvPIP2-1* and *VvPIP2-2* were the most prominently expressed isogenes, with mRNA levels approximately 4- to 32-fold greater than the other isogenes (Fig. 4C). *VvPIP2-1* and *VvPIP2-2* mRNA levels were 16-fold or more greater in the cortex and stele than in the exodermis, a pattern shared by *VvPIP2-3*. There were no significant differences in mRNA levels between tissues for *VvPIP2-4*.

In the maturation zone, sections were dissected into six tissues: the exodermis, cortex, endodermis, pericycle and phloem (at this stage of development, these tissues could not be reliably differentiated, so they were combined), xylem, and central stele (Fig. 4D). Within the maturation zone, *VvPIP1-1* was the only *VvPIP1* family member with significant differences in mRNA levels between tissues, with the greatest levels in the exodermis, endodermis, and xylem tissues and the lowest levels in the central stele (Fig. 4E). Within the *VvPIP2* family, *VvPIP2-2* and *VvPIP2-3* mRNA levels varied significantly between tissues, with both of these isogenes having peak mRNA levels in the endodermis, pericycle/phloem, and xylem tissues (Fig. 4F).

In the secondary growth zone of the root, sections were also dissected into six tissues: the exoderm, cortex, periderm, pericycle, phloem, and xylem (Fig. 4G). The state of the outer cell layers was variable in this zone, sometime being present and intact and sometimes being in some state of dissolution as the outer cell layers were lost. *VvPIP* expression was undetected in these outer cell layers (Fig. 4, H and I). Within this growing zone, all isogenes had the greatest mean levels of expression in phloem and xylem tissues, with lower levels of expression in the pericycle and periderm (Fig. 4, H and I). Within the *VvPIP1* family, *VvPIP1-1* was the most prominently expressed isogene in the periderm, with *VvPIP1-2;1-4* being the most prominently expressed

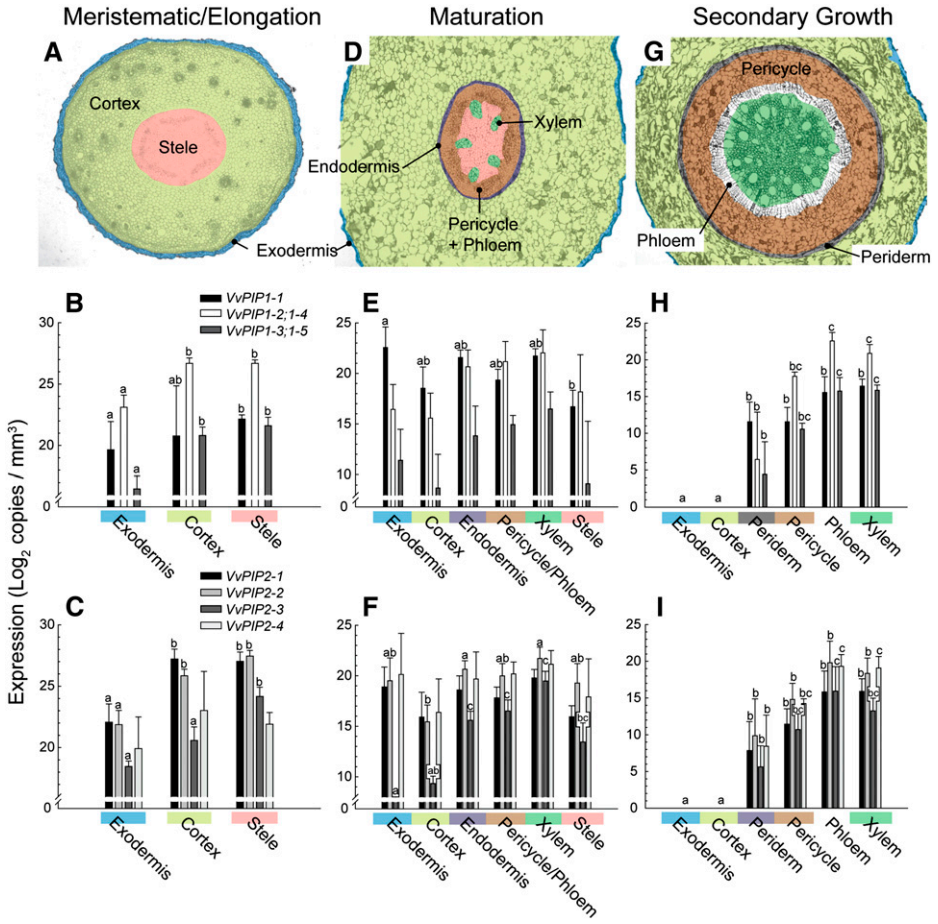

Figure 4. Tissue-specific expression patterns of *Vitis* species aquaporin isogenes. A to C, Expression of *VvPIP1* (B) and *VvPIP2* (C) family aquaporins in the meristematic and elongation zones within three tissues: exodermis (blue), cortex (yellow), and stele (pink). D to F, Expression of *VvPIP1* (E) and *VvPIP2* (F) family aquaporins in the maturation zone within six tissues: epidermis (blue), cortex (yellow), endodermis (purple), combined pericycle and phloem (brown), xylem (green), and pith (pink). G to I, Expression of *VvPIP1* (H) and *VvPIP2* (I) family aquaporins in the secondary growth zone within six tissues: exodermis (blue), cortex (yellow), periderm (gray), pericycle (brown), phloem (white), and combined xylem and pith (green). Error bars represent SE, and different letters represent significant differences between tissues within individual isogenes (n = 3–5; Tukey's honestly significant difference[HSD], $P < 0.05$).

isogene in other tissues (Fig. 4H). Within the *VvPIP2* family, mRNA levels were equivalent among isogenes within each tissue (Fig. 4I).

Longitudinal Patterns of *VvPIP* Expression

Tissue-specific mRNA levels for the *VvPIP* isogenes also varied significantly longitudinally along the length of the root, decreasing from peak levels in the meristematic and elongation zones to lower levels in more distal root zones (Fig. 4, compare B with E and H and C with F and I; note the difference in scale). For example, *VvPIP1-2* was expressed at levels nearly 100-fold lower (Fig. 4, B, E, and H) and *VvPIP2* isogenes were expressed at levels 4- to 64-fold lower (Fig. 4, C and F) in older root zones. *VvPIP* mRNA levels in the periderm were on the order of 2^{10} copies mm^{-3}, compared with values that ranged from 2^{15} to 2^{25} copies mm^{-3} (as much as a greater than 10,000-fold difference) in the maturation and meristematic/elongation zones.

Comparisons with the Arabidopsis Root

We compared the patterns of *VvPIP* expression characterized above with those of orthologous Arabidopsis (*Arabidopsis thaliana*) genes from the work of Brady et al. (2007; Fig. 5). This analysis served to summarize the data presented here while providing a comparison with the only other quantitative analysis of gene expression within specific root tissues. The protein sequences of eight Arabidopsis *PIP* isogenes represented on the microarray utilized by Brady et al. (2007) were clustered with the VvPIPs (Fig. 5A). All the AtPIP1 proteins clustered with VvPIP1-1. Within the PIP2s, AtPIP2-1 and AtPIP2-3 clustered with VvPIP2-1 and VvPIP2-4, AtPIP2-8 clustered with VvPIP2-2, and AtPIP2-6 and VvPIP2-3 were more divergent proteins. Longitudinally, both the Arabidopsis (Fig. 5B) and *Vitis* species (Fig. 5C) isogenes had peak mRNA levels in the meristematic and elongation zones and much lower levels of expression in the maturation zone. In *Vitis* species, mRNA levels dropped further in the secondary growth zone (Fig. 5C), which is absent in the herbaceous Arabidopsis root. On average, *VvPIP* mRNA levels decreased approximately 100-fold between the meristematic and elongation and secondary growth zones. For radial expression patterns in the meristematic and elongation zones, both the Arabidopsis and *Vitis* species isogenes had peak mRNA levels in the cortex and stele, with much lower expression levels in the exodermis, with the exception of *AtPIP2-8* (Fig. 5D). In the maturation

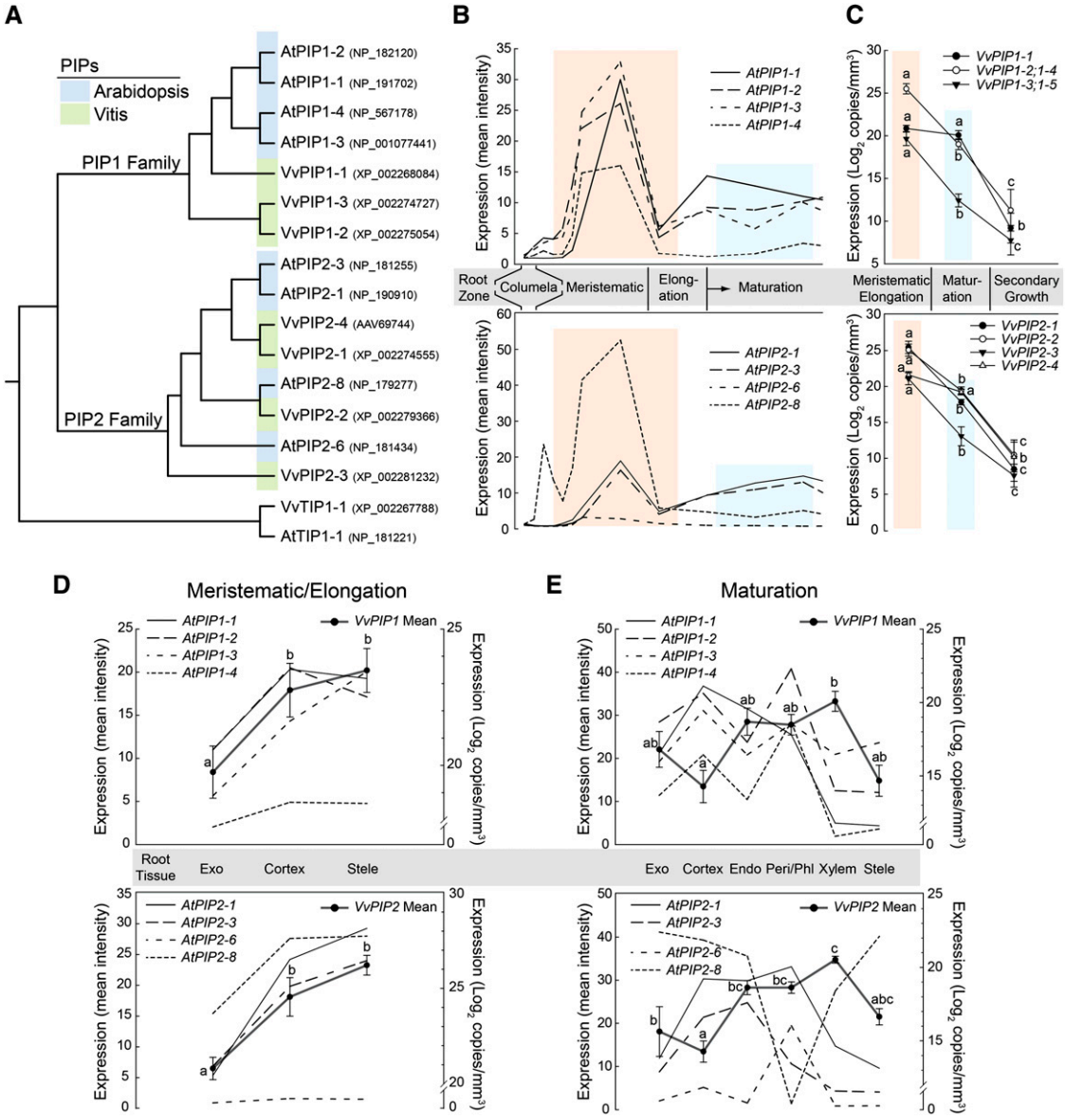

Figure 5. Relationships between tissue-specific expression patterns of Arabidopsis and *Vitis* species aquaporin genes in fine roots. A, Rooted dendrogram illustrating the relationships between various PIP isoforms in Arabidopsis (blue) and *Vitis* species (green). The tree is rooted with AtTIP1-1 and VvTIP1-1. National Center for Biotechnology Information protein accession numbers are given. B and C, Longitudinal expression patterns of individual *PIP* isogenes in Arabidopsis (B) and *Vitis* species (C). Similar root zones in either species are highlighted: meristematic and elongation zones (pink) and the maturation zone (blue). D and E, Radial expression patterns in Arabidopsis (lines) and *Vitis* species (thick lines) in both the meristematic and elongation zones (D) and the maturation zone (E). *Vitis* species *PIP* expression is present as a mean of all isogenes within a family for ease of presentation. Error bars represent SE, and different letters represent significant differences between tissues (n = 9–15; Tukey's HSD, $P < 0.05$).

zone, the patterns of expression were highly variable. There were few similarities within the *PIP1* family except for peak mRNA levels in the pericycle and phloem tissues and relatively low levels in the central stele (Fig. 5E). Within the *PIP2* family, both species exhibited lower levels of expression in the exodermis, cortex, and stele, with higher levels in the endodermis and pericycle/phloem, except for the anomalous pattern of *AtPIP2-8* (Fig. 5E). Generally, *Vitis* species had high levels of all *PIPs* in the xylem, in contrast to all *AtPIPs* except for *AtPIP2-8*.

DISCUSSION

This study characterizes dramatic changes in anatomy, suberization, and hydraulic physiology along the

root length, and the roots analyzed here exhibited a secondary growth zone with a multilayer, highly suberized periderm, which cannot be found in herbaceous roots. The highest levels of Lp_r were associated with increased aquaporin protein activity (i.e. under osmotically driven flow) and peak *VvPIP* expression levels occurring in the root tip. Radially, *VvPIP* expression was always greatest in interior tissues (i.e. stele, endodermis, and/or vascular tissues). Lp_r was at least10-fold less in the secondary growth zone as compared with the root tip, and low levels of *VvPIP* expression and protein activity in the secondary growth zone suggest that the *VvPIP*s do not play a prominent role in controlling radial water uptake in suberized woody root portions, counter to the expectations of Steudle (2000). Despite having much lower Lp_r, suberized roots were not completely sealed and can constitute the vast majority of the root system surface area in mature grapevines, thus still providing potentially significant water uptake under field conditions.

Developmental Anatomy and Lp_r

Our data demonstrate that changes in root anatomy alone had profound effects on Lp_r. Under conditions when aquaporin activity was maximal (i.e. for noninhibited roots), Lp_r was much lower in the secondary growth zone than in the meristematic/elongation zone. This coincided with the development of a suberized periderm and low aquaporin activity. Even when aquaporin activity was inhibited, Lp_r^{Os} and Lp_r^{Hy} were both 14-fold lower in the secondary growth zone compared with the root tip. Based on a comparison of Lp_r^{Os} and Lp_r^{Hy} (Lp_r^{Hy} is 100-fold greater than Lp_r^{Os}) within the secondary growth zone, the apoplastic pathway was identified as the predominant pathway across the root, similar to findings for Lupin roots by Bramley et al. (2009). In the secondary root zone, aquaporin inhibition had no effect on Lp_r^{Hy}, and only under $\Delta\Psi^{Os}$ did aquaporins contribute Lp_r (5%). Hence, lower overall Lp_r in the secondary growth zone is likely caused by the suberized periderm; similar relationships between the presence of a developed periderm and decreases in Lp_r have been described in desert species (North and Nobel, 1995, 1996). It is interesting that the formation of the suberized periderm does not completely seal the apoplastic pathway for the secondary growth zone, as suggested by Steudle (2000).

The most intensely studied suberized apoplastic barrier is the suberized Casparian band of the endodermis. Evidence that the Casparian band impedes solute transport is long standing (Esau, 1977), but the extent to which suberization impacts Lp_r is not as well characterized. Physical puncturing of the endodermis in corn (*Zea mays*) roots increases the root's reflection coefficient (i.e. solute permeability) but has negligible effects on Lp_r (Steudle et al., 1993). Recent studies showed that enhanced aliphatic suberin content in Arabidopsis mutants (i.e. twice the amount of suberin as the wild type) failed to reduce Lp_r, while a mutant with a slower rate of development of suberized structures and 33% less suberin exhibited higher water permeability (Ranathunge and Schreiber, 2011). It was concluded from this study that not only does the content matter but also the composition of the suberin and its microstructure for the formation of apoplastic barriers. Suberization patterns of the exodermis and periderm differ from the endodermis in two regards: (1) additional suberization of one or both periclinal walls (although suberization of one periclinal wall sometimes occurs in the endodermis of older root portions in some herbaceous species; Esau, 1977); and (2) the presence of multiple suberized cell layers (Esau, 1977). In barley (*Hordeum vulgare*), Sanderson (1983) showed that the extent of suberization of the interior periclinal walls of the endodermis is extremely well correlated with decreases in Lp_r. In corn, the presence of a suberized exodermis (single cell layer) leads to a nearly 4-fold reduction of Lp_r (Zimmermann and Steudle, 1998; Zimmermann et al., 2000). The results presented here suggest that suberized apoplastic barriers decrease Lp_r to an equal or even greater extent.

Water Uptake along the Root

The majority of water uptake in roots is most often attributed to the fine unsuberized root tips. In this study, the root tip had Lp_r^{Os} and Lp_r^{Hy} that were approximately 14-fold greater compared with the secondary growth zone. We did not measure Lp_r of the maturation zone in this study, but in a previous study the Lp_r^{Os} and Lp_r^{Hy} of root lengths that included the root tip and maturation zone were intermediate between the root tip and secondary growth portion Lp_r found here (Gambetta et al., 2012). The relative contribution of the secondary growth zone increases over multiple growth seasons. Queen (1967) found that heavily suberized *Vitis* species roots from previous growing seasons were 5 times less water permeable than current season roots. Although older suberized portions of roots have much lower Lp_r, they constitute a much greater proportion of the total root system surface area and, therefore, provide significant potential for water uptake (Kramer and Bullock, 1966; Queen, 1967; Chung and Kramer, 1975; MacFall et al., 1990, 1991).

Based on our root hydraulic conductance results, we created a simple model to conceptualize the relative contributions of the tip and secondary growth portions to total water flow. In one scenario, root conductance scales linearly with root length, while in the other, there is a decrease in conductance with root length (Supplemental Fig. S2). For any root, increased tip size increases its relative contribution (Supplemental Fig. S3). In a short fine root (less than 10 cm), most of the water uptake would indeed be localized to the root tip regardless of tip size or conductance scaling. As root length increases, differences in tip size and changes in

conductance can lead to large differences in the relative contributions of root portions. When the tip is small, the proportion of water flowing through the tip decreases rapidly with root length. In a woody perennial rooting system, this simple model illustrates how phenological (i.e. root tip flushes) and developmental (i.e. formation of suberized cell layers) changes can alter patterns of uptake across a growing season. After fine root flushes when tips would be relatively large, unsuberized, and permeable, uptake through root tips would predominate, but this relationship could change dramatically under conditions that promote suberization (e.g. water deficit commonly used in viticulture; Vandeluer et al., 2009).

This heterogeneity of Lp_r along the length of the root may be one of the factors that contribute to the observed high variability of Lp_r between roots with similar appearance (Gambetta et al., 2012). Even if one were to consider single fine roots of given length and diameter (i.e. equal total surface areas), the relative surface areas of different root portions will differ, perhaps substantially, leading to variability in Lp_r of the whole root. This is well illustrated by Ranathunge and Schreiber (2011), who showed that Arabidopsis mutants with a delay in the rate of development of suberized structures had significantly greater Lp_r. Presumably, the difference in Lp_r resulted from a greater proportion of the mutant root length being unsuberized and, thus, imparting a greater Lp_r to the root as a whole. Differences in Lp_r along the root length represent a tradeoff between the potential for water uptake and water loss. High Lp_r allows for higher rates of water uptake but also higher rates of water loss under dry conditions (Richards and Caldwell, 1987). This tradeoff has given rise to the idea of root sealing, where the Lp_r of older root portions would decrease to near zero, eliminating any potential for water loss and to facilitate uptake by root tips (Zwieniecki et al., 2002). This and many other studies discussed above have demonstrated that roots do not become completely "sealed," although in this study we did find rare secondary root portions that had Lp_r^{Os} and Lp_r^{Hy} values near zero. The combination of high Lp_r of the actively growing root portion and a sharp decrease in Lp_r with the initiation of secondary growth results in the contribution of root portions being relative to the size of growth, an idea previously explored by Zwieniecki et al. (2002).

Aquaporin Localization and Lp_r

We found significant differences in the localized magnitude of *VvPIP* mRNA levels and aquaporin protein activity within *Vitis* species fine roots. Longitudinally, both *VvPIP* mRNA and the contribution of aquaporin protein activity to Lp_r were greatest in root tips. Expression levels for all *VvPIP* isogenes were approximately 100- to 1,000-fold greater in the meristematic and elongation zones than in more proximal root portions (Fig. 4C), a result consistent with previous studies in our laboratory (Gambetta et al., 2012) and in situ hybridization studies of Vandeleur et al. (2009) for *VvPIP1-1* and *VvPIP2-2* and of Perrone et al. (2012) for *VvPIP2-4*. Across other plant species, numerous aquaporin isogenes also exhibit far greater levels of expression in root tips than in more distal root portions, including *PIPs* in Arabidopsis (Fig. 4, A–C; Brady et al., 2007), tobacco (*Nicotiana tabacum*; Otto and Kaldenhoff, 2000), and corn (Hachez et al., 2006).

Radially, the *VvPIP*s had significant levels of expression across all tissues along the length of the root, with the exception of the deteriorating outer cell layers coincident with the initiation of secondary growth (Figs. 1 and 3). For many isogenes, peak mRNA levels were associated with the undifferentiated stele in the meristematic and elongation zones and more interior tissues, including the endodermis (maturation zone only), pericycle, and vascular tissues in the maturation and secondary growth zones (Otto and Kaldenhoff, 2000; Suga et al., 2003; Fraysse et al., 2005; Vandeleur et al., 2009; Knipfer et al., 2011). While our data here represent mRNA levels only, there is a striking congruence between aquaporin mRNA and protein abundance in studies that have localized both in roots (Otto and Kaldenhoff, 2000; Hachez et al., 2006; Vandeleur et al., 2009). Furthermore, the longitudinal patterns of *VvPIP* expression characterized here are strongly correlated with the contribution of aquaporin activity to Lp_r (discussed below).

It is important to consider that, in this study, *VvPIP* expression was determined from tissues isolated using LCM. LCM is a powerful tool allowing for the isolation of specific tissues. However, the amount of tissue isolated via LCM represents a very small percentage of the total tissue in a root, and there is a danger that this could lead to sampling bias. The high congruence of the results here with those of other studies suggests that this was not the case.

High mRNA levels in the meristematic and elongation zones corresponded to an approximately 45% contribution of aquaporin protein activity to Lp_r^{Os}. In the secondary growth zone, mean *VvPIP* mRNA levels were approximately 1,000-fold lower and corresponded to a scant approximately 5% contribution to Lp_r^{Os}. A similar pattern was found for Lp_r^{Hy}, with a 5% contribution in the meristematic and elongation zones and no contribution in the secondary growth zone. The contribution of aquaporins to Lp_r across species (for review, see Javot and Maurel, 2002) is highly variable, and results from our laboratory on fine root portions (above) as well as whole *Vitis* species fine roots (Gambetta et al., 2012) have exhibited contributions to Lp_r^{Hy} ranging from 0% to 67% in individual roots or root portions, a result similar to the range found in other *Vitis* species (Lovisolo et al., 2008).

In this study, the data demonstrate a strong correlation between *VvPIP* expression and aquaporin activity; nevertheless, they suggest that aquaporins do not play a large role in water uptake under conditions

of active transpiration (i.e. under a predominantly $\Delta\Psi^{Hy}$) in *Vitis* species roots. The most straightforward explanations for the small contribution of aquaporins to Lp_r^{Hy} are as follows: (1) an apoplastic pathway is predominant under $\Delta\Psi^{Hy}$; (2) apoplastic barriers do not provide for great enough changes in the resistance of the apoplast to force a significant amount of flow across cell membranes; and/or (3) those cells across which flow is forced do not contain high levels of aquaporin activity in their membranes. Indeed, in the secondary growth zone, a location where flow would theoretically be forced across cell membranes due to suberized barriers would be the periderm, a tissue exhibiting the lowest *VvPIP* mRNA levels of any measured (Figs. 2 and 3). Counter to our findings here, Hachez et al. (2012) found that aeroponically grown corn roots develop an exodermis with Casparian bands and exhibit increased levels of ZmPIP2;5 and ZmPIP1;2 in this tissue. They argue that increased aquaporin expression helps to compensate for the increased resistance in this portion of the apoplastic pathway. These patterns may differ between woody perennial and herbaceous rooting systems.

It is possible that the contribution of aquaporins reported here could be underestimated due to incomplete inhibition. Traditionally, mercuric chloride inhibitors have been used in aquaporin inhibition experiments, but this inhibitor has high toxicity and the inability to inhibit some aquaporin isoforms (Daniels et al., 1994; Biela et al., 1999; Krajinski et al., 2000). Alternative chemical inhibition has been shown to be equally effective as mercuric chloride in many studies (Henzler et al., 2004; Ye and Steudle, 2006; McElrone et al., 2007). Incomplete inhibition could result from limited penetration of the inhibitor into root tissues. This seems unlikely in root tip portions, evidenced by the lack of suberized structures and the high level of inhibition under $\Delta\Psi^{Os}$. However, it is possible that tissue penetration may be more problematic in the secondary root zone due to the presence of the suberized periderm (Barrowclough et al., 2000; Martre et al., 2001).

In extending information on mRNA quantity and localization, it is important to consider that impacts on Lp_r (this is even true for semiquantitative protein localization) are difficult due to the complex nature of aquaporin heterotetramerization. Experiments in *Xenopus laevis* oocytes show that many PIP1 proteins are often hydraulically inactive and PIP2 proteins increase membrane water permeability, while coexpression of particular *PIP1* and *PIP2* isoforms can increase membrane hydraulic permeability far above the levels measured with the expression of those genes alone; a similar interaction was also found for *VvPIP*s (Vandeleur et al., 2009). Four PIP1 E-loop residues are critical for facilitating the heterotetramerization of PIP isoforms, increasing the hydraulic function of PIP1 isoforms (Fetter et al., 2004). The VvPIP1s in our study share 100% similarity across these residues (as reported by Choat et al. [2009]).

When patterns of *VvPIP* expression were compared with those found in the Arabidopsis root (Fig. 4), there were striking similarities, especially considering the taxonomic distance between the two species. Furthermore, peak expression in the meristematic/elongation zone is a pattern curiously shared across many species. One explanation would be that high aquaporin levels in the root tip, and a greater contribution of aquaporin activity to Lp_r, enable the plant to have greater and more rapid control over Lp_r in a region of the root where a majority of water uptake and continued growth occurs. This seems reasonable for herbaceous species, but if aquaporins were to play a consistent role in the control of tissue- and organ-level hydraulics, then why would aquaporin gene expression and protein activity decrease so abruptly upon the transition to more mature root tissues, especially in the case of woody roots, where substantial water uptake can occur in older woody root portions (MacFall et al., 1990)? Another plausible explanation is that the primary biological purpose of aquaporins is not aimed at influencing tissue- and organ-level hydraulics. It may be that aquaporins do alter the bulk permeability of the tissues where they have high activity, but their primary purpose is to facilitate cell-level water relations in tissues undergoing rapid growth and/or solute exchange, namely the meristematic and elongation zones of the root tip and vascular tissues. Other studies have proposed similar hypotheses, that aquaporins play a critical role in regulating source-sink relationships (Schäffner, 1998; Suga et al., 2003; Fraysse et al., 2005).

CONCLUSION

Here, we characterized anatomical, molecular, and biophysical aspects of fine roots impacting water uptake in *Vitis* species, a woody perennial. This study provides one of the few quantitative analyses of tissue-specific aquaporin expression in roots and, to our knowledge, the first in a woody species. This study reveals strong parallels in developmental anatomy, the distribution of aquaporins, and relationships with Lp_r between herbaceous and woody fine roots within the meristematic/elongation and maturation zones. These similarities suggest that a common foundation likely underlies the integration of root development and water uptake across plants.

MATERIALS AND METHODS

Plant Material and Growth Conditions

The commonly utilized rootstock 110R (grapevine [*Vitis berlandieri* × *Vitis rupestris*]) was used in all experiments and was rooted from green cuttings obtained from the University of California, Davis, experimental vineyards. Vines were potted into a modified University of California soil mix (one-third peat, one-third sand, and one-third redwood compost, supplemented with dolomite lime) in 4.3-L pots. Plants were grown under greenhouse conditions for 6 to 8 weeks prior to conducting the root experiments. Plants were drip

irrigated daily with water supplemented with calcium (90 μg mL^{-1}), magnesium (24 μg mL^{-1}), potassium (124 μg mL^{-1}), nitrogen as NH_4 (6 μg mL^{-1}), nitrogen as NO_3 (96 μg mL^{-1}), phosphorus (26 μg mL^{-1}), sulfur (16 μg mL^{-1}), iron (1.6 μg mL^{-1}), manganese (0.27 μg mL^{-1}), copper (0.16 μg mL^{-1}), zinc (0.12 μg mL^{-1}), boron (0.26 μg mL^{-1}), and molybdenum (0.016 μg mL^{-1}) at pH 5.5 to 6.0. The plants were grown under a constant photoperiod with temperatures ranging from 20°C to 25°C.

Sampling, Tissue Preparation, and Light Microscopy

Root sampling occurred between 8 and 10 AM. Vines were brought to the laboratory and carefully removed from pots, growing medium was carefully washed from the roots, and razor blades were used to cut healthy fine roots from the root mass under water. For paraffin embedding, root portions were cut into small pieces (approximately 1 mm thick) and fixed immediately in ice-cold 75% ethanol and 25% acetic acid. For cryosectioning, the small pieces were immediately placed into O.C.T. Compound (Tissue-Tek, Sakura Finetek). Berberine hemisulfate, analine blue staining was carried out on fresh hand sections as described by Choat et al. (2009). For Lp_r measurements, root portions were cut under water and transferred to deionized water, and experiments were carried out immediately.

For light microscopy, tissues were fixed under vacuum for 4 h. Tissues were then dehydrated at 4°C with a 75%, 85%, 95%, and 100% ethanol series, 2 to 4 h for each step. After dehydration, ethanol was intermediated with Hemo-De (3:1, 1:1, and 1:3 ethanol:Hemo-De with 2 h for each step followed by 100% Hemo-De twice), and then tissues were infiltrated with a Hemo-De-paraffin mixture at 42°C for 4 h. The solution was then replaced with 100% paraffin at 60°C, and tissues were infiltrated at 60°C for 2 d with several changes of paraffin. After infiltration with paraffin, tissues were embedded into paraffin blocks and stored at 4°C shortly before microtome sectioning. Embedded tissues were cut into 10-μm-thick sections using a Microm HM 310 microtome (Thermo Scientific). Sections were mounted onto Superfrost Plus microscope slides (Fisher Scientific) and dried for 0.5 h at 42°C followed by 1 h at room temperature. Slides were stained with 0.05% toluidine blue O (in deionized water) for 10 min and then rinsed with deionized water. Slides were left at room temperature until dry, and paraffin was removed with Hemo-De for 2 min and mounted with Permount toluene solution (Fisher Scientific). Bright- and dark-field microscopy was carried out on a Zeiss Axioskop2 plus microscope (Carl Zeiss), and images were captured using an AxioCam digital camera (Carl Zeiss) and accompanying software.

LCM

LCM was performed on tissues that were fixed and sectioned in two different ways: paraffin embedding and cryosectioning. Both methodologies were used to ensure that the fixation, embedding, and sectioning method itself were not biasing subsequent mRNA quantification. For LCM, paraffin-embedded tissues were prepared as described above with the caveats that all water used in the protocol was double autoclaved and treated with 0.05% diethyl pyrocarbonate (DEPC; Sigma-Aldrich), all glassware was rinsed with 0.1% fresh DEPC water and then dried in the oven, and the microtome, water bath, warm tray, and other tools used during microtome sectioning were cleaned with RNaseZap (Ambion) and double-autoclaved DEPC-treated water. The tissues were cut into 10-μm-thick sections and mounted onto RNase-free PEN-membrane slides (Leica; catalog no. 11505189). The slides were dried and paraffin was removed as described above. Slides were stored at 4°C, and LCM was carried out within 5 d to ensure high RNA quality.

For cryosectioning, samples in O.C.T. Compound (Tissue-Tek, Sakura Finetek) were placed into RNase-free cryomolds, frozen in liquid nitrogen, and stored at −80°C until sectioning. The cryostat was cleaned with 100% ethanol prior to sectioning, and other tools and surfaces in contact with the tissue were cleaned with RNaseZap (Ambion). The root tissues were cut into 10-μm-thick sections at −20°C and mounted onto the RNase-free PEN-membrane slides (Leica). Thirty microliters of prechilled RNAlater-ICE (Ambion) was pipetted directly onto each section. The slides were stored flat at −20°C overnight. The following day, the slides were rinsed with RNase-free water for 4 min and desiccated until dry at room temperature (about 10 min). LCM was carried out immediately.

Different parts of the root tissue (e.g. epidermis, cortex, endodermis, etc.) were dissected by using the Leica LMD 6000 LCM microscope (Supplemental Fig. S1). Tissues were cut into the cap of a 0.5-mL RNase-free PCR tube containing 30 μL of RNAqueous Lysis buffer (RNAqueous-Micro kit; Ambion). After tissue capture was complete, the PCR tube was removed, the contents were spun down briefly, and the sample was frozen at −80°C until RNA isolation. Biological replication (different roots from different plants) was three to five times depending on the tissue.

RNA Isolation and Quantitative PCR

RNA was isolated from the LCM tissues using the RNAqueous-Micro kit (Ambion) with minor modification for DNase treatment. (DNA was treated by using the Qiagen RNase-Free DNase Set following the wash of Wash Solution 1. After DNase treatment for 30 min at 37°C, the column was washed with Wash Solution 1 and the protocol was continued according to the manufacturer's instructions.) RNA was eluted from the column using 2 × 10 μL of Elution Solution (RNAqueous-Micro kit; Ambion). RNA was quantified and quality assessed using an Agilent 2100 BioAnalyzer (Agilent Technologies). Approximately 5 ng of RNA was reverse transcribed using the methods described by Choat et al. (2009), and *VvPIP* mRNA levels were absolutely quantified using genomic DNA standards as described by Gambetta et al. (2010, 2012) with one modification. In this study, LCM isolation of tissues allows for the precise quantification of the tissue volume from which RNA is isolated. Therefore, we expressed mRNA levels as the number of copies per mm^3 of tissue. All samples were run in duplicate.

With regard to the quantification of the *VvPIP* isogenes, it is important to point out that researchers have difficulty resolving some isogenes (i.e. whether multiple extremely closely related complementary DNAs represent allelic variants, true isogenes, or possibly the same gene in the case of partial complementary DNAs; Supplemental Table S1). This is discussed in more detail by Gambetta et al. (2012). Here, we report expression levels as *VvPIP1-2;1-4* and *VvPIP1-3;1-5* for these putative isogenes/allelic variants.

Comparison of Quantitative PCR Data with Arabidopsis Data

The tissue-specific expression data for the Arabidopsis (*Arabidopsis thaliana*) plasma membrane aquaporins were obtained from the supplemental data of Brady et al. (2007; available at http://www.sciencemag.org/content/318/5851/801/suppl/DC1). Those Arabidopsis plasma membrane aquaporin isogenes represented in the top 50% of varying genes were used in the analysis (Brady et al., 2007). Protein sequences for these genes were obtained through the National Center for Biotechnology Information and were clustered with the VvPIP proteins (ClustalW, BLOSUM matrix with gap open penalty of 10 and gap extension penalty of 1; rooted with the AtTIP1 and VvTIP1 proteins), producing rooted dendrograms (Fig. 4A).

Radial and longitudinal expression patterns for the *AtPIPs* were obtained from supplemental table S12 in Brady et al. (2007). Root zone designations for the Arabidopsis data were taken from figure 1 in Brady et al. (2007) after discussion with those authors. For longitudinal comparisons, the expression levels of individuals were averaged across all tissues within a given root zone. For radial comparisons, the expression levels of all isogenes within a *VvPIP* family were averaged within a given root zone and tissue.

Measures of Hydraulic Conductance

Lp_r was measured in fine roots using two different methods depending on the driving force, as described previously (Gambetta et al., 2012). Briefly, for experiments using a hydrostatic pressure gradient, a meniscus tracking method was used. Root tips or secondary growth portions were excised under water and prepared immediately for Lp_r measurements. Root portions were sealed into a luer fitting using nontoxic, dental impression polymer (Pentron Clinical Technologies). For root tips, the first 10 to 20 mm including the tip was used. Secondary root portions (typically 10–20 mm in length) did not contain any lateral roots, and the distal open end was sealed. Both root diameter and root length were measured and recorded, from which surface area was later calculated. Seals were tested for each sample prior to taking measurements. Samples were then connected to tubing fed through the lid of a pressure chamber (Soil Moisture Equipment) and submersed in diH_2O inside the pressure chamber. The tube protruding from the lid was connected to a microcapillary that was used to measure outflow from the sample by tracking the movement of a meniscus at the air-water interface. A range of pressures was used (0.1–0.3 MPa; a minimum of four 0.03- to 0.05-MPa pressure steps). Control Lp_r values were first obtained with the root submersed in diH_2O, and then measurements were repeated with

0.6 mM hydrogen peroxide for aquaporin chemical inhibition. Hydrogen peroxide-based solutions have been used effectively as inhibitors of aquaporin activity while providing lower toxicity than mercuric chloride (Henzler et al., 2004; Ye and Steudle, 2006; McElrone et al., 2007). Lp_r (m s^{-1} MPa^{-1}) was calculated using the following equation: $Lp_r = (Qv/P)(1/A)$, where Qv/P (m^3 s^{-1} MPa^{-1}) is the slope of the pressure flow relationship across the different hydrostatic pressures and A (m^2) is the root surface area. These Lp_r measurements were completed within 45 min after excision for each sample, and we found no evidence for decreasing Lp_r values over this time period.

Axial hydraulic conductance was measured in an identical experiment to that described above, only root portions were sequentially cut under water. In the case of root tips, cuts were made sequentially beginning at the root apex, and pressure flow relationships were measured after each cut. Within the meristematic and elongation zones (prior to the development of primary xylem; see above), axial hydraulic conductance was equal to intact root Lp_r (data not shown). In the maturation and secondary growth zones, axial hydraulic conductance was 100 to 1,000 times greater than Lp_r. Thus, Lp_r reflects the radial Lp_r, since the axial resistance is relatively negligible (0.1%–1% of total resistance).

For experiments using an osmotic pressure gradient, root portions were prepared as described above and glued into a 500-μm-diameter glass capillary. The capillary and root were fed into a custom-made chamber (Gambetta et al., 2012), and flow through the root was quantified as above. Roots were equilibrated for at least 1 h in diH_2O followed by measurements of flow in Suc solutions of various osmotic strengths (0, 0.125, 0.25, and 0.5 MPa). In some cases, measurements were replicated on the same root using both Suc and mannitol solutions of equal osmotic strengths with no difference in the resulting Lp_r. The root was allowed to equilibrate in each solution for at least 30 min, and flows were stable. There was no evidence for decreasing Lp_r values over time (i.e. values were linear across the solutions). Aquaporin inhibition was then carried out immediately on the same root as described above.

Statistical Analyses

All statistical analyses were carried out using SAS software (SAS Institute; http://www.sas.com). ANOVAs were carried out, and means were compared using Tukey's HSD for multiple pairwise comparisons, in the case of mRNA levels, or Student's t test, in the case of Lp_r.

Supplemental Data

The following materials are available in the online version of this article.

Supplemental Figure S1. An example of LCM cuts made on a section of a secondary growth root portion; not all cuts are shown.

Supplemental Figure S2. Simple model used to conceptualize the relative contribution of fine root tips to total water uptake along the length of a root.

Supplemental Figure S3. Simple model used to conceptualize the relative contribution of fine root tips to total water uptake along the length of a root as described in Supplemental Figure S2.

Supplemental Table S1. Primer pair sequences used in this study.

Received May 13, 2013; accepted September 12, 2013; published September 18, 2013.

LITERATURE CITED

Barrowclough DE, Peterson CA, Steudle E (2000) Radial hydraulic conductivity along developing onion roots. J Exp Bot **51:** 547–557

Biela A, Grote K, Otto B, Hoth S, Hedrich R, Kaldenhoff R (1999) The *Nicotiana tabacum* plasma membrane aquaporin NtAQP1 is mercury-insensitive and permeable for glycerol. Plant J **18:** 565–570

Brady SM, Orlando DA, Lee JY, Wang JY, Koch J, Dinneny JR, Mace D, Ohler U, Benfey PN (2007) A high-resolution root spatiotemporal map reveals dominant expression patterns. Science **318:** 801–806

Bramley H, Turner NC, Turner DW, Tyerman SD (2009) Roles of morphology, anatomy, and aquaporins in determining contrasting hydraulic behavior of roots. Plant Physiol **150:** 348–364

Choat B, Gambetta GA, Shackel KA, Matthews MA (2009) Vascular function in grape berries across development and its relevance to apparent hydraulic isolation. Plant Physiol **151:** 1677–1687

Chung HH, Kramer PJ (1975) Absorption of water and ^{32}P through suberized and unsuberized roots of loblolly pine. Can J For Res **5:** 229–235

Daniels MJ, Mirkov TE, Chrispeels MJ (1994) The plasma membrane of *Arabidopsis thaliana* contains a mercury-insensitive aquaporin that is a homolog of the tonoplast water channel protein TIP. Plant Physiol **106:** 1325–1333

Esau K (1977) Anatomy of Seed Plants, Ed 2. Wiley, New York

Fetter K, Van Wilder V, Moshelion M, Chaumont F (2004) Interactions between plasma membrane aquaporins modulate their water channel activity. Plant Cell **16:** 215–228

Fraysse LC, Wells B, McCann MC, Kjellbom P (2005) Specific plasma membrane aquaporins of the PIP1 subfamily are expressed in sieve elements and guard cells. Biol Cell **97:** 519–534

Gambetta GA, Manuck CM, Drucker ST, Shaghasi T, Fort K, Matthews MA, Walker MA, McElrone AJ (2012) The relationship between root hydraulics and scion vigour across Vitis rootstocks: what role do root aquaporins play? J Exp Bot **63:** 6445–6455

Gambetta GA, Matthews MA, Shaghasi TH, McElrone AJ, Castellarin SD (2010) Sugar and abscisic acid signaling orthologs are activated at the onset of ripening in grape. Planta **232:** 219–234

Hachez C, Moshelion M, Zelazny E, Cavez D, Chaumont F (2006) Localization and quantification of plasma membrane aquaporin expression in maize primary root: a clue to understanding their role as cellular plumbers. Plant Mol Biol **62:** 305–323

Hachez C, Veselov D, Ye Q, Reinhardt H, Knipfer T, Fricke W, Chaumont F (2012) Short-term control of maize cell and root water permeability through plasma membrane aquaporin isoforms. Plant Cell Environ **35:** 185–198

Hallgren SW, Rudinger M, Steudle E (1994) Root hydraulic-properties of spruce measured with the pressure probe. Plant Soil **167:** 91–98

Henzler T, Ye Q, Steudle E (2004) Oxidative gating of water channels (aquaporins) in Chara by hydroxyl radicals. Plant Cell Environ **27:** 1184–1195

Javot H, Maurel C (2002) The role of aquaporins in root water uptake. Ann Bot (Lond) **90:** 301–313

Knipfer T, Besse M, Verdeil JL, Fricke W (2011) Aquaporin-facilitated water uptake in barley (*Hordeum vulgare* L.) roots. J Exp Bot **62:** 4115–4126

Knipfer T, Fricke W (2011) Water uptake by seminal and adventitious roots in relation to whole-plant water flow in barley (*Hordeum vulgare* L.). J Exp Bot **62:** 717–733

Krajinski F, Biela A, Schubert D, Gianinazzi-Pearson V, Kaldenhoff R, Franken P (2000) Arbuscular mycorrhiza development regulates the mRNA abundance of Mtaqp1 encoding a mercury-insensitive aquaporin of *Medicago truncatula*. Planta **211:** 85–90

Kramer PJ, Boyer JS (1995) Water relations of plants and soil. Academic Press, Inc., San Diego, CA

Kramer PJ, Bullock HC (1966) Seasonal variations in proportions of suberized and unsuberized roots of trees in relation to absorption of water. Am J Bot **53:** 200–204

Lovisolo C, Tramontini S, Flexas J, Schubert A (2008) Mercurial inhibition of root hydraulic conductance in *Vitis* spp. rootstocks under water stress. Environ Exp Bot **63:** 178–182

MacFall JS, Johnson GA, Kramer PJ (1990) Observation of a water-depletion region surrounding loblolly pine roots by magnetic resonance imaging. Proc Natl Acad Sci USA **87:** 1203–1207

MacFall JS, Johnson GA, Kramer PJ (1991) Comparative water-uptake by roots of different ages in seedlings of loblolly-pine (*Pinus taeda* L). New Phytol **119:** 551–560

Martre P, North GB, Nobel PS (2001) Hydraulic conductance and mercury-sensitive water transport for roots of *Opuntia acanthocarpa* in relation to soil drying and rewetting. Plant Physiol **126:** 352–362

McElrone AJ, Bichler J, Pockman WT, Addington RN, Linder CR, Jackson RB (2007) Aquaporin-mediated changes in hydraulic conductivity of deep tree roots accessed via caves. Plant Cell Environ **30:** 1411–1421

Miyamoto N, Steudle E, Hirasawa T, Lafitte R (2001) Hydraulic conductivity of rice roots. J Exp Bot **52:** 1835–1846

Nightingale GT (1934) Effects of temperature on growth, anatomy, and metabolism of apple and peach roots. Bot Gaz **96:** 581–639

North GB, Nobel PS (1995) Hydraulic conductivity of concentric root tissues of *Agave deserti* Engelm under wet and drying conditions. New Phytol **130:** 47–57

North GB, Nobel PS (1996) Radial hydraulic conductivity of individual root tissues of *Opuntia ficus-indica* L. Miller as soil moisture varies. Ann Bot (Lond) **77:** 133–142

Oparka KJ, Prior DAM (1992) Direct evidence for pressure-generated closure of plasmodesmata. Plant J **2:** 741–750

Otto B, Kaldenhoff R (2000) Cell-specific expression of the mercury-insensitive plasma-membrane aquaporin NtAQP1 from *Nicotiana tabacum*. Planta **211:** 167–172

Perrone I, Gambino G, Chitarra W, Vitali M, Pagliarani C, Riccomagno N, Balestrini R, Kaldenhoff R, Uehlein N, Gribaudo I, et al (2012) The grapevine root-specific aquaporin VvPIP2;4N controls root hydraulic conductance and leaf gas exchange under well-watered conditions but not under water stress. Plant Physiol **160:** 965–977

Peterson CA, Enstone DE (1996) Functions of passage cells in the endodermis and exodermis of roots. Physiol Plant **97:** 592–598

Peterson CA, Murrmann M, Steudle E (1993) Location of the major barriers to water and ion movement in young roots of *Zea-mays* L. Planta **190:** 127–136

Queen WH (1967) Radial movement of water and ^{32}P through suberized and unsuberized roots of grape. PhD thesis. Duke University, Durham, NC

Ranathunge K, Schreiber L (2011) Water and solute permeabilities of *Arabidopsis* roots in relation to the amount and composition of aliphatic suberin. J Exp Bot **62:** 1961–1974

Richards JH, Caldwell MM (1987) Hydraulic lift: substantial nocturnal water transport between soil layers by *Artemisia tridentata* roots. Oecologia **73:** 486–489

Roberts AG, Oparka KJ (2003) Plasmodesmata and the control of symplastic transport. Plant Cell Environ **26:** 103–124

Sanderson J (1983) Water-uptake by different regions of the barley root: pathways of radial flow in relation to development of the endodermis. J Exp Bot **34:** 240–253

Schäffner AR (1998) Aquaporin function, structure, and expression: are there more surprises to surface in water relations? Planta **204:** 131–139

Schreiber L, Franke R, Hartmann KD, Ranathunge K, Steudle E (2005) The chemical composition of suberin in apoplastic barriers affects radial hydraulic conductivity differently in the roots of rice (*Oryza sativa* L. cv. IR64) and corn (*Zea mays* L. cv. Helix). J Exp Bot **56:** 1427–1436

Steudle E (2000) Water uptake by roots: effects of water deficit. J Exp Bot **51:** 1531–1542

Steudle E (2001) The cohesion-tension mechanism and the acquisition of water by plant roots. Annu Rev Plant Physiol Plant Mol Biol **52:** 847–875

Steudle E, Murrmann M, Peterson CA (1993) Transport of water and solutes across maize roots modified by puncturing the endodermis: further evidence for the composite transport model of the root. Plant Physiol **103:** 335–349

Steudle E, Oren R, Schulze ED (1987) Water transport in maize roots: measurement of hydraulic conductivity, solute permeability, and of reflection coefficients of excised roots using the root pressure probe. Plant Physiol **84:** 1220–1232

Suga S, Murai M, Kuwagata T, Maeshima M (2003) Differences in aquaporin levels among cell types of radish and measurement of osmotic water permeability of individual protoplasts. Plant Cell Physiol **44:** 277–286

Vandeleur RK, Mayo G, Shelden MC, Gilliham M, Kaiser BN, Tyerman SD (2009) The role of plasma membrane intrinsic protein aquaporins in water transport through roots: diurnal and drought stress responses reveal different strategies between isohydric and anisohydric cultivars of grapevine. Plant Physiol **149:** 445–460

Ye Q, Steudle E (2006) Oxidative gating of water channels (aquaporins) in corn roots. Plant Cell Environ **29:** 459–470

Zimmermann HM, Hartmann K, Schreiber L, Steudle E (2000) Chemical composition of apoplastic transport barriers in relation to radial hydraulic conductivity of corn roots (*Zea mays* L.). Planta **210:** 302–311

Zimmermann HM, Steudle E (1998) Apoplastic transport across young maize roots: effect of the exodermis. Planta **206:** 7–19

Zwieniecki MA, Thompson MV, Holbrook NM (2002) Understanding the hydraulics of porous pipes: tradeoffs between water uptake and root length utilization. J Plant Growth Regul **21:** 315–323